Analytical investigation of non-adiabatic effects on the dynamics of sound reflection and transmission in a combustor

S. M. Hosseinalipour[1*], A. Fattahi[1], N. Karimi[2]

[1]School of Mechanical Engineering, Iran University of Science and Technology, Tehran, Iran

[2]School of Engineering, University of Glasgow, Glasgow G12 8QQ, United Kingdom

* Corresponding author: alipour@iust.ac.ir

Abstract

Acoustics of a simplified, non-adiabatic combustor chamber, including a duct followed by a downstream exit nozzle, are considered. This system features heat transfer to the environment and, therefore involves mean axial temperature gradient along the duct and the nozzle. The effect of heat transfer on the dynamics of the acoustic reflection and transmission in the duct and nozzle is investigated analytically. These involve development of analytical expressions for the response of non-adiabatic nozzles through compact acoustic modelling and also the effective length approach. Further, an existing work on the dynamics of heat transferring ducts is extended and combined with that of the nozzles. The acoustic responses of the combined non-adiabatic system are, subsequently, characterized by analyzing the net reflection and transmission of an incident acoustic wave. The results show that heat transfer can considerably modify the dynamic behavior of the acoustic reflections and transmissions. Due to the multiple reflections in the system, the phase response features significant irregularities. It is argued that the observed modifications in the chamber acoustics can noticeably affect the thermoacoustics of the system.

Keywords: Sound reflection; sound transmission; thermoacoustic response; combustor and nozzle system.

1. Introduction

The rapidly increasing concerns about the environmental impacts of power generation sector have led to imposing stringent emission regulations [1,2]. These regulations require gas turbine and aero-engine manufacturers to achieve very low levels of NO_x emissions [2]. It is well demonstrated that lean premixed combustion technology is most efficient in reducing NO_x formation in modern gas turbine combustors [2,3]. However, the high susceptibility of premixed flames to thermoacoustic instabilities has, so far, hindered the wide application of this combustion technology [1,3]. Thermoacoustic instabilities are the result of complex interactions between the flame heat release and combustion chamber acoustics [4,5]. Occurrence of these instabilities can lead to the generation of coherent, large amplitude pressure oscillations [1, 2]. In a gas turbine combustor, these can induce strong mechanical vibrations and increase the heat transfer rates and, therefore damage the system severely [1,2].

Over the last few decades, there have been sustained efforts for understanding and suppression of thermoacoustic instabilities in various combustion systems, see Refs. [2-5] for reviews of the literature. Nonetheless, due to the substantial complexity of the thermoacoustic instabilities, they are still not fully understood [1,5]. Thus, the accurate prediction of these requires solving the fluid flow and combustion governing equations through the prohibitively expensive computations [5, 6]. The more practical approach to the problem of thermoacoustic

modelling is through the so-called "low order modelling" [7]. This approach is on the basis of the classical theory of control and essentially divides the system into two major dynamical, mutually interacting sub-systems [8]. The system dynamics are then analysed by the conventional black box method [9]. The sub-systems, or black boxes represent the flame dynamics and the chamber acoustics [4]. The former is often characterised through the experimental measurements [10,11], numerical simulations [12-14] or theoretical calculations [15]. The latter, however, is usually approximated by solving the quasi one-dimensional Euler equations in the combustion chamber [8]. A linear stability analysis is then conducted to explore the stability limits of the system [7-9]. Low order models of thermoacoustic systems include considerable simplifications and even have been fundamentally criticised [16]. Nonetheless, the practical feasibility of using low order models has turned them into an attractive choice for industry [2,7,8]. This has led to major attempts to improve these models through advancement of the combustion and acoustics sub-models. For instance, nonlinearities were included in the sub-models of flame dynamics by the introduction of flame describing functions [17]. Similarly, the acoustic sub-models of combustor were significantly refined [7]. Particularly in recent years, improving the analytical modelling of the acoustic boundary conditions has received a considerable attention [18-20].

The problem of acoustic reflection and transmission is, generally, of importance in combustor acoustics [2,7]. This is due to the significant effects of the reflections on the thermoacoustic stability of combustors and the pertinence of the acoustic transmissions to the problem of combustion noise [1]. In particular, the correct prediction of the amplitude and phase of the acoustic reflections is central to the accurate stability analysis of combustors [7, 21]. Further, the characteristics of the acoustic transmission directly affect the noise emission of the system [22,23]. It follows that incorporation of all the physical mechanisms capable of modifying the acoustic reflection and transmission, is a key step in improving the acoustic models of combustors. This will be, in turn, an important contribution to the development of more accurate, low order, thermoacoustic models.

In general, any changes in the impedance of the propagation medium can cause reflection of the acoustic waves [24]. Considering the Euler equations as the theoretical framework, two principle mechanisms can be identified for the acoustic reflections in a combustor. These include modifications of the cross sectional area and changes in the flow density induced by the temperature variations. The first mechanism is active around the exit nozzle of the combustor. Modelling tools for the inclusion of this mechanism include the well-known model of Marble and Candel [25], as well as several recent extensions of this model [18-20,26]. The second mechanism, however, has received much less attention and, in fact, is currently being widely ignored by most thermoacoustic models. Nevertheless, so far, there have been very limited evaluations of the effects of mean temperature variations upon the chamber acoustics.

Acoustics of inhomogeneous, density varying, media were analysed theoretically in the past, see for example Refs. [27,28]. In the context of thermoacoustics, Sujith et al. [29] investigated the acoustics of a duct with axial mean temperature variations and zero mean flow. They considered a prescribed distribution of the axial mean temperature along the duct and developed analytical solutions for the resultant inhomogeneous wave equation [29]. Their one-dimensional results were, then, validated against experiments [29]. This work was later extended to the cases with nonlinear temperature distributions [30,31], and finite mean temperature and particulate damping [31,32]. These studies were intended to describe the acoustics of the combustors under heat transferring condition, in which there were variations in the axial mean temperature. However, they all expressed spatio-temporal pressure and velocity

perturbations and did not provide explicit information on the dynamics of the acoustic reflections and transmissions. This issue was resolved by Karimi et al. [33], in their analysis of frequency response of the disturbance and acoustic energy of a heat transferring duct. These authors showed that the variations in the axial mean temperature could cause significant, frequency dependent reflections [33]. The amplitude and phase response of this reflection were argued to be of importance in the thermoacoustics of the system [33].

In reality, the combustor duct and the exit nozzle both feature heat transfer. As a result of heat transfer, the mean temperature of the flow in both of these two components can decline. This introduces a reflection mechanism, which interacts with that induced by the variations in the cross-sectional areas [34]. Hence, the net acoustic reflection and transmission is due to the accumulative effects of heat transfer and cross-sectional changes [34]. Given the high sensitivity of thermoacoustic stability upon the dynamics of acoustic reflections, it is essential to predict these combined effects most accurately. As stated earlier, currently, there exist advanced models of acoustic reflections and transmissions from isothermal nozzles [18-20]. There have been also few attempts to express the acoustics of heat transferring ducts [29,33,34]. However, the acoustics of non-adiabatic nozzles, with temperature varying flows, remain entirely unexplored. Further, so far, there has been no study on the dynamics of acoustic reflections and transmissions in a system of duct and exit nozzle, featuring heat transfer and cross-sectional variations.

The current work aims to address these issues and improve the current state of combustor acoustic modelling through the followings. First, it provides novel analytical models for the dynamics of acoustic reflection and transmission in heat transferring nozzles. These include compact models for low frequency limits, as well as phase responses through utilisation of the concept of effective length. Second, it extends the previous works on the heat transferring ducts to nonlinear axial temperature distributions. Finally, it combines the two effects of heat transfer and area variations in a combustion chamber, consisting of a duct and an exit nozzle, and finds the acoustic reflection and transmission coefficients.

2. Theoretical analysis

2. 1. Problem configuration

Fig. 1 shows the schematic view of the problem under investigation. It includes a convergent-divergent nozzle attached at the exit of a straight duct. Variation of the gas density in the duct, induced by the temperature change, and also modification of the cross sectional area in the nozzle alter the acoustic impedance of the system [7]. This causes reflections of the acoustic waves in the duct and nozzle [3, 33]. An acoustic incident wave (ε) enters the combustor and this generates reflected (P_c^-) and transmitted (P_c^+) acoustic waves. The transmitted wave propagates into the nozzle, while the reflected wave travels towards upstream section, which is an infinitely long duct. The transmitted wave generally produces three acoustic waves in the nozzle; $P_{1,n}^-$, $P_{2,n}^+$ and $P_{2,n}^-$. In here, indices 1 and 2 represent the upstream and downstream of the nozzle throat, respectively. Further, n and c subscripts denote combustor and nozzle waves. In addition, + and – symbols indicate the waves travelling towards the downstream and upstream of the mean flow.

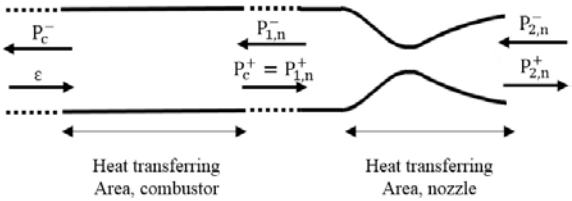

Fig. 1. Schematic view of the combustor and nozzle.

The proceeding analysis include the following assumptions;
(a) the working fluid is inviscid, non-heat-conducting ideal gas.
(b)the heat transfer is purely radiative and unsteady heat transfer is negligible,
(c) cooling does not change the critical statue of the nozzle,
(d) there is no shock wave in the divergent part of the supercritical nozzle,
(e) the mean flow and wave are one-dimensional and there is no friction losses,
In the current work, the divergent section of the non-compact nozzle is ten times longer than that of the convergent section. As Table 1 illustrates [35], the area ratio is chosen such that the outlet Mach numbers do not change in the selected inlet Mach numbers.

Table 1- The inlet and outlet Mach numbers and area ratios of the adiabatic nozzle from Ref. [35]

		Unchoked	Choked
		$M_{n,2} = 0.4$	$M_{n,2} = 1.2$
$M_{n,1} = 0.05$	A_1/A^*	*7.310*	*11.695*
	A_2/A^*	*1.000*	*1.032*
$M_{n,1} = 0.1$	A_1/A^*	*3.671*	*5.873*
	A_2/A^*	*1.000*	*1.032*

The details of the investigated cases study are provided in Tables 2 to 4 for the compact and non-compact cases. In these tables, θ is the ratio of the fluid stagnation temperature at the outlet to the inlet.

Table2- The compact cases

Nozzle regime		$M_{n,1}$
Subcritical	Case 1	0.1
	Case 2	0.05
Supercritical	Case 3	0.1
	Case 4	0.05

Table3- The non-compact cases

Nozzle regime		$M_{n,1}$	Overall θ
Subcritical	Case 5	0.1	0.7
	Case 6	0.05	0.7
	Case 7	0.1	0.85
	Case 8	0.05	0.85
Supercritical	Case 9	0.1	0.7
	Case 10	0.05	0.7
	Case 11	0.1	0.85
	Case 12	0.05	0.85

Table4- Thermal conditions of the combustor and nozzle

θ_c	θ_n	Overall θ
0.7	0.9	0.63
0.73	0.91	0.66
0.76	0.92	0.7
0.79	0.93	0.73
0.82	0.94	0.77
0.85	0.95	0.81
0.88	0.96	0.84
0.91	0.97	0.88
0.94	0.98	0.92
0.97	0.99	0.96
1	1	1

2.2. Heat transfer effects

2.2.1. Compact nozzle

Considering the assumptions stated in section 2.1, the one-dimensional conservation equations of mass, momentum and energy are

$$\frac{1}{\rho}\left(\frac{\partial \rho}{\partial t}+u\frac{\partial \rho}{\partial x}\right)+\frac{\partial u}{\partial x}=0, \tag{1}$$

$$\frac{\partial u}{\partial t}+u\frac{\partial u}{\partial x}+\frac{1}{\rho}\frac{\partial p}{\partial x}=0, \tag{2}$$

$$\frac{D\rho}{Dt}=\frac{\rho}{\gamma p}\left(\frac{Dp}{Dt}-(\gamma-1)q\right). \tag{3}$$

In Eqs. (1-3), p, ρ, u and t are respectively the static pressure (Pa), fluid density (kg/m^3), velocity (m/s) and time (s). q is the heat loss per unit volume (W/m^3). Equations (1-3) constitute the Euler equations and therefore do not include heat and momentum diffusion effects. It should be noted that the use of Euler equations for describing combustor acoustics is common practice, see Refs. [2,7,18,19].

Flow variable are then substituted by the summation of the steady and disturbance parts. That is $g=\bar{g}+g'$, in which g is a flow property and $\bar{g}$, g' represent respectively, the time averaging and perturbation components. Ignoring the second order terms results in the linearized mass, momentum and energy equations of (1)-(3). These are

$$\left(\frac{\partial}{\partial t}+\bar{u}\frac{\partial}{\partial x}\right)\frac{\acute{\rho}}{\bar{\rho}}+\bar{u}\frac{\partial}{\partial x}\left(\frac{\acute{u}}{\bar{u}}\right)=0, \tag{4}$$

$$\frac{\partial}{\partial t}\left(\frac{\acute{u}}{\bar{u}}\right)+\bar{u}\frac{\partial}{\partial x}\left(\frac{\acute{u}}{\bar{u}}\right)+\frac{\acute{\rho}}{\bar{\rho}}\frac{\partial \bar{u}}{\partial x}+2\bar{\rho}\bar{u}\frac{\acute{u}}{\bar{u}}\frac{\partial \bar{u}}{\partial x}+\bar{p}\frac{\partial}{\partial x}\left(\frac{\acute{p}}{\bar{p}}\right)+\frac{\acute{p}}{\bar{p}}\frac{\partial \acute{p}}{\partial \bar{p}}=0, \tag{5}$$

$$\frac{D}{Dt}\left(\frac{p'}{\overline{\gamma p}}+\frac{\rho'}{\bar{\rho}}\right)=\frac{\bar{q}R}{\bar{p}}\left(\frac{q'}{\bar{q}}-\frac{u'}{\bar{u}}-\frac{p'}{\bar{p}}\right). \tag{6}$$

Combining Eqs. (4) and (6) yields

$$\left(\frac{\partial}{\partial t}+\bar{u}\frac{\partial}{\partial x}\right)\left(\frac{\acute{p}}{\gamma \bar{p}}\right)+\bar{u}\frac{\partial}{\partial x}\left(\frac{u'}{\bar{u}}\right)=\frac{\bar{q}R}{\bar{p}}\left(\frac{q'}{\bar{q}}-\frac{u'}{\bar{u}}-\frac{p'}{\bar{p}}\right). \tag{8}$$

The acoustic waves are assumed to be the planar propagating waves in both directions of the one-dimensional domain. Thus,

$$\frac{p'}{\gamma\bar{p}} = P^{+}\,exp\left(i\omega\left[t-\frac{x}{\bar{u}+c}\right]\right) + P^{-}\,exp\left(i\omega\left[t-\frac{x}{\bar{u}-c}\right]\right), \quad (9)$$

$$\frac{u'}{c} = U^{+}\,exp\left(i\omega\left[t-\frac{x}{\bar{u}+c}\right]\right) + U^{-}\,exp\left(i\omega\left[t-\frac{x}{\bar{u}-c}\right]\right), \quad (10)$$

in which ω is the angular frequency. Relations (9) and (10) are applied to the homogenous flow regions, located immediately upstream or downstream of the nozzle.
Through substitution of the harmonic distribution for pressure, velocity and heat flux into Eqs. (4) and (8), the following expressions can be developed,

$$\rho^{+} = U^{+}, \quad (11\text{-a})$$

$$\rho^{-} = -U^{-}, \quad (11\text{-b})$$

$$U^{+} = P^{+}, \quad (11\text{-c})$$

$$U^{-} = -P^{-}, \quad (11\text{-d})$$

$$q^{+} = P^{+}\left(\gamma+\frac{1}{M}\right) + P^{-}\left(\gamma-\frac{1}{M}\right). \quad (11\text{-e})$$

Conservation of mass in the nozzle results in

$$\frac{1}{M}\left(\frac{\acute{u}}{c}\right) + \frac{\rho'}{\bar{\rho}} = \text{const.} \quad (12)$$

Because of the heat transfer effects on acoustic waves, an energy balance should be introduced. This reads

$$\dot{q} = \dot{m}C_p(T_{t2} - T_{t1}), \quad (13)$$

where $T_t, \dot{m}$ and $\dot{q}$ are the stagnation temperature, mass flow rate and heat transfer rate. Linearizing Eq. (13) and considering $\left(\frac{\acute{\dot{m}}}{\bar{\dot{m}}}\right)_1 = \left(\frac{\acute{\dot{m}}}{\bar{\dot{m}}}\right)_2$ [35] for the two parts of the nozzle reveals that

$$\frac{\acute{T}_{t1}}{\bar{T}_{t1}} + \frac{\acute{q}}{\bar{\dot{m}}C_p\bar{T}_{t1}} = \frac{\acute{T}_{t2}}{\bar{T}_{t2}}\left(1+\frac{1}{B}\right) + \frac{1}{B}\frac{\acute{\dot{m}}}{\bar{\dot{m}}}. \quad (14)$$

As mentioned before, q is the heat transfer per unit volume and

$$q = \frac{\dot{m}}{V}C_p\Delta T_t = \frac{\rho_1 u_1}{\frac{V}{A}}C_p\Delta T_t. \quad (15)$$

By linearizing Eq. (15), the heat transfer fluctuation can be expressed as

$$\frac{q'}{\bar{q}} = A\frac{T'_{t2}}{\bar{T}_{t2}} - B\frac{T'_{t1}}{\bar{T}_{t1}} + \frac{\rho'_1}{\bar{\rho}_1} + \frac{u'_1}{\bar{u}_1}, \quad (16\text{-a})$$

in which

$$A = -\frac{\bar{T}_{t2}}{\bar{T}_{t2}-\bar{T}_{t1}}, \quad (16\text{-b})$$

$$B = -\frac{\bar{T}_{t1}}{\bar{T}_{t2}-\bar{T}_{t1}}. \quad (16\text{-c})$$

The stagnation temperature is

$$T_t = T\left(1+\frac{\gamma-1}{2}M^2\right) \quad (17)$$

Linearization of this yields

$$\frac{\acute{T}_t}{\overline{T}_t} = \frac{1}{1+\frac{1}{2}(\gamma-1)M^2}\left[\gamma\left(\frac{p'}{\gamma\overline{p}}\right) - \frac{\acute{\rho}}{\rho} + (\gamma-1)\frac{M\acute{u}}{c}\right] = \frac{1}{1+\frac{1}{2}(\gamma-1)M^2}\left[(\gamma-1)\left(\frac{p'}{\gamma\overline{p}}\right) - \frac{\acute{s}}{c_p} + (\gamma-1)\frac{M\acute{u}}{c}\right]. \quad (18)$$

Heat transfer modifies the Mach number at the outlet of a conduit with a constant cross section [36]. Expectedly, the variation of Mach number through a heat transferring conduit with variable area section (e.g. a nozzle) differs from that of a constant area conduit traditionally presented by Rayleigh line [37]. Considering the nozzle geometry, inlet condition and variation of the stagnation temperature, the outlet Mach number of the nozzle can be found by an iterative method [37]. The inlet Mach number of the combustor is then calculated by Rayleigh line [37].

Here, the acoustic response of a heat transferring nozzle to an incident acoustic wave by the strength of ${P_1}^+$ is analysed. Considering Eqs. (11) and (12) in the subcritical regime, a relation among the transmitted acoustic wave in the diverging part and the acoustic components in the converging section is derived. This is

$${P_{n,2}}^+ = \frac{1}{M_{n,1}(1+M_{n,2})}\left[M_{n,2}\left({P_{n,1}}^+ - {P_{n,1}}^-\right) + M_{n,1}M_{n,2}\left({P_{n,1}}^+ + {P_{n,1}}^-\right)\right]. \quad (19)$$

In the subcritical nozzle, there is no acoustic wave in the downstream section and thus, ${P_{n,2}}^-$ is assumed to be zero. Combining Eqs. (11), (16) and (18) gives

$${P_{n,1}}^- = \frac{{K_1}^+}{{K_1}^-}{P_{n,1}}^+, \quad (20\text{-a})$$

where

$${K_1}^+ = -B\left(1+\frac{1}{2}(\gamma-1){M_2}^2\right)(\gamma-1)(1+M_1) + A\left(1+\frac{1}{2}(\gamma-1){M_1}^2\right)(\gamma-1)\left(\frac{M_2}{M_1} + M_2\right) + \left(1+\frac{1}{2}(\gamma-1){M_1}^2\right)\left(1+\frac{1}{2}(\gamma-1){M_2}^2\right)\left(\frac{-(\gamma M_2+1)}{M_1(1+M_2)} - \frac{(\gamma M_2+1)}{(1+M_2)} + (\gamma-1)\right), \quad (20\text{-b})$$

$${K_1}^- = B\left(1+\frac{1}{2}(\gamma-1){M_2}^2\right)(\gamma-1)(1-M_1) + A\left(1+\frac{1}{2}(\gamma-1){M_1}^2\right)(\gamma-1)\left(\frac{M_2}{M_1} - M_2\right) + \left(1+\frac{1}{2}(\gamma-1){M_1}^2\right)\left(1+\frac{1}{2}(\gamma-1){M_2}^2\right)\left(\frac{(\gamma M_2+1)}{(1+M_2)} - \frac{(\gamma M_2+1)}{M_1(1+M_2)} + (\gamma-1)\right). \quad (20\text{-c})$$

The transmitted acoustic wave in the downstream section is found by substituting Eq. (20-a) into Eq. (19), which gives

$${P_{n,2}}^+ = \frac{1}{M_{n,1}(1+M_{n,2})}\left[M_{n,2}\left(1-\frac{{K_1}^+}{{K_1}^-}\right) + M_{n,1}M_{n,2}\left(1+\frac{{K_1}^+}{{K_1}^-}\right)\right]{P_{n,1}}^+. \quad (21)$$

In the supercritical regime, relations derived by Marble and Candel [25] are still valid. These are

$${P_{n,1}}^- = \frac{1-\frac{1}{2}(\gamma-1)M_1}{1+\frac{1}{2}(\gamma-1)M_1}{P_{n,1}}^+, \quad (22)$$

$${P_{n,2}}^+ = \frac{1+\frac{1}{2}(\gamma-1)M_2}{1+\frac{1}{2}(\gamma-1)M_1}{P_{n,1}}^+, \quad (23)$$

$${P_{n,2}}^- = \frac{1-\frac{1}{2}(\gamma-1)M_2}{1+\frac{1}{2}(\gamma-1)M_1}{P_{n,1}}^+. \quad (24)$$

However, the outlet Mach number should be now calculated with the consideration of heat transfer effect. It is also worth noting that Eqs. (22)-(24) are not limited to adiabatic flows and remain equally valid for the current hear exchanging flows [25].

2.2.2. Non-compact nozzle

This section extends the analysis of non-adiabatic flow to non-compact nozzles. Similar to Ref. [19], the concept of "effective length" is utilized here. Effective length approximates a nozzle

with two connected conduits without any change in cross sectional area (Fig. 2). Each conduit has its own length as an effective length.

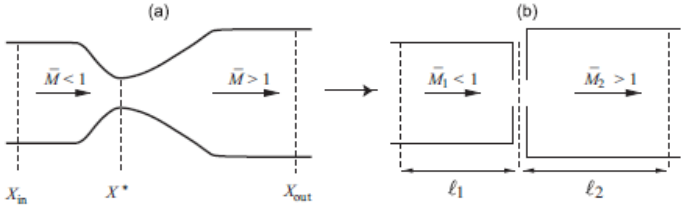

Fig. 2. (a) A convergent-divergent nozzle (b) Equivalent conduits of constant cross sectional areas rendering the effective lengths.

To find the effective length, the linearized equations of mass, momentum and energy (Eqs. (4), (5) and (6)) are considered. Dimensionless, harmonic, flow perturbations may be written as

$$\frac{p'}{\gamma\bar{p}} = \hat{p}(X)e^{i\omega t}\ ,\ \frac{\rho'}{\bar{\rho}} = \hat{\rho}(X)e^{i\omega t}\ ,\ \frac{u'}{\bar{u}} = \hat{u}(X)e^{i\omega t}, \tag{25}$$

in which $X = x/l$ and l is the axial nozzle length.

In a choked nozzle, Mach number and the dimensionless perturbation frequency may be presented with respect to the flow velocity at the throat (i.e. sound speed c). Thus,

$$M^* = \frac{\bar{u}}{c^*},\ \Omega_n = \frac{\omega l}{c^*}$$

in which, the superscript * denotes the throat of a choked nozzle, Ω_n is the dimensionless frequency (Strouhal number) and subscript n denotes nozzle.

After removal of the steady flow component and using the dimensionless perturbation, the mass conservation equation is written as [19]

$$i\Omega_n\hat{\rho} + M^*\left(\frac{d\hat{u}}{dX} + \frac{d\hat{\rho}}{dX}\right) = 0. \tag{26}$$

The energy equation reduces to

$$i\Omega_n(\hat{p} - \hat{\rho}) + M^*\left(\frac{d\hat{p}}{dX} + \frac{d\hat{\rho}}{dX}\right) = M^*\frac{\Delta T_t}{\bar{T}}(\hat{q} - \hat{p} - \hat{u}). \tag{27}$$

Further, conservation of the total enthalpy in the mean flow results in

$$\bar{c}^2 = \frac{c^{*2}}{2}(\gamma + 1) - \frac{\bar{u}^2}{2}(\gamma + 1) + \bar{Q}(\gamma - 1). \tag{28}$$

It should be noted that the unit of $\bar{q}$ in Eq. (3) is W/m^3. However, the unit of $\bar{Q}$ in Eq. (28) is J/kg. Thus,

$$\bar{Q} = \bar{q}\frac{V}{\dot{m}} = c_p\Delta T_t. \tag{29}$$

Employing Eqs. (28) and (29), the momentum equation becomes

$$i\Omega_n\hat{u} + M^*\frac{d\hat{u}}{dX} + \frac{dM^*}{dX}(2\hat{u} + \hat{\rho} - \gamma\hat{p}) + \frac{1}{2}\frac{d\hat{p}}{dX}\left[\frac{\gamma+1}{M^*} - (\gamma - 1)M^* + \frac{2c_p\Delta T_t}{M^*c^{*2}}(\gamma - 1)\right] = 0. \tag{30}$$

An algebraic manipulation of Eqs. (26), (27) and (30) reveals

$$\begin{aligned} i\Omega_n\left[M^*(2\hat{u} + \hat{\rho} - \hat{p}) - \frac{1}{M^*}(\hat{\rho} + \hat{p})\right] + \frac{d}{dX}\left[\left(M^{*2} - 1\right)(2\hat{u} + \hat{\rho} - \gamma\hat{p})\right] + \\ \frac{d\hat{p}}{dX}\frac{2c_p\Delta T_t}{c^{*2}}(\gamma - 1) + \left(M^{*2} - 1\right)\frac{\Delta T_t}{\bar{T}}(\hat{q} - \hat{p} - \hat{u}) = 0. \end{aligned} \tag{31}$$

Flow perturbations may be presented by the following asymptotic expansions

$$\hat{p} = \hat{p}_0 + i\Omega_n\hat{p}_1 + O\left(\Omega_n{}^2\right) \tag{32-a}$$

$$\hat{\rho} = \hat{\rho}_0 + i\Omega_n\hat{\rho}_1 + O\left(\Omega_n{}^2\right) \tag{32-b}$$

$$\hat{u} = \hat{u}_0 + i\Omega_n\hat{u}_1 + O\left(\Omega_n{}^2\right) \tag{32-c}$$

By substituting Eq. (32) into Eq. (31), the boundary conditions of a choked nozzle for the zeroth order are derived. These are

$$2\hat{u}_0 + \hat{\rho}_0 - \gamma\hat{p}_0 = 0, \tag{33}$$

$$\hat{q}_0 - \hat{u}_0 - \hat{p}_0 = 0. \tag{34}$$

Due to neglecting the higher order terms, Eqs. (32a-c), Eqs. (33) and (34) are valid for a compact nozzle. Eq. (33) had first derived by Stow et al. [38] and was verified by Goh and Morgans [19]. It is noted that Eq. (34) is essentially the same as Eq. (12).

The first order of asymptotic expansion of Eq. (31) is integrated. This reveals

$$\begin{aligned}\left[(M^{*2}-1)(2\hat{u}_1+\hat{\rho}_1-\hat{p}_1)\right]_{X_1}^{X_2} = (\hat{\rho}_0+\hat{p}_0)\int_{X_1}^{X_2}\frac{dX}{M^*} - (2\hat{u}_0+\hat{\rho}_0-\hat{p}_0)\int_{X_1}^{X_2}M^*dX - \\ 2(\gamma-1)c_p\Delta T_t\int_{X_1}^{X_2}\frac{M^{*2}}{\bar{u}^2}d\hat{p}_1 - \int_{X_1}^{X_2}\frac{\Delta T_t}{\bar{T}}\left(M^{*2}+1\right)(\hat{q}_1-\hat{p}_1-\hat{u}_1)dX.\end{aligned} \tag{35}$$

By using Eq. (35) in the range of $X = X_{in}$ to $X = X^*$and consideration of $\bar{c} = \sqrt{\gamma R\bar{T}}$ and $\frac{c_p}{\gamma R}(\gamma-1) = 1$, the effective length of the convergent part is found as follows,

$$l_1 = \int_{X_{in}}^{X^*}\frac{\bar{M}_{n,1}}{\bar{M}_n}\sqrt{\frac{1+\frac{\gamma-1}{2}\bar{M}^2-\frac{\Delta T_{t1}}{\bar{T}}}{1+\frac{\gamma-1}{2}\bar{M}_0{}^2-\frac{\Delta T_{t1}}{\bar{T}_1}}}dX. \tag{36}$$

in which $\bar{T}_1$ and $\bar{T}_{t1}$are mean and stagnation inlet temperature, respectively, and $\Delta T_{t1} = T^* - T_{t1}$. It should be noted that due to $M^* \ll 1$ in deriving Eq. (35), the terms including the multiplication of M^* can be neglected compared to those including $1/M^*$.

For the divergent part, Eq. (35) should be implemented between $X = X^*$ and $X = X_{out}$. In accordance with Eq. (33), the effective length of the divergent part is obtained as

$$l_2 = \frac{2\hat{p}_0\int_{X_{in}}^{X^*}\frac{1}{M^*}dX-(\gamma-1)\hat{p}_0\int_{X_{in}}^{X^*}M^*dX}{\frac{(\hat{p}_0+\hat{\rho}_0)}{M^*{}_{n,2}}-(\gamma-1)\hat{p}_0M^*{}_{n.2}}, \tag{37}$$

where $M^*{}_{n,2}$ is the outlet nozzle Mach number which can be rewritten with accordance to the first law of thermodynamics,

$$M_{n,2}{}^* = \sqrt{\frac{\frac{\gamma+1}{2}}{1+\frac{\gamma-1}{2}\bar{M}^2-\frac{\Delta T_{t2}}{\bar{T}_2}}}. \tag{38}$$

Duran and Moreaue [26] showed that indirect noise source prevails only at low frequencies. Hence, to assess the entropy noise, the values of $\hat{p}_0+\hat{\rho}_0$ and $\hat{p}_0$ are substituted from the results of the compact nozzle in section of 2.2.1. The nozzle response to acoustic waves are

$$\frac{P_2^+}{P_1^+} = \left|\frac{P_2^+}{P_1^+}\right| e^{ik_2^+l_2+ik_1^+l_1} + O\left(\Omega_n{}^2\right), \tag{39}$$

$$\frac{P_2^-}{P_1^+} = \left|\frac{P_2^-}{P_1^+}\right| e^{ik_2^-l_2+ik_1^+l_1} + O\left(\Omega_n{}^2\right), \tag{40}$$

in which $k_2^+ = \omega/(\bar{c}_2+\bar{u}_2)$, $k_2^- = \omega/(\bar{c}_2-\bar{u}_2)$ and $k_1^+ = \frac{\omega}{\bar{c}_1+\bar{u}_1}$.

2.2.3.Non-compact combustor

Sujith et al. [29] showed that in a duct with zero mean flow and axial temperature gradient, the acoustic wave equation can be written as

$$\frac{d^2P'}{dx^2} + \frac{1}{\bar{T}}\frac{d\bar{T}}{dx}\frac{dP'}{dx} + \frac{\omega^2}{\gamma R\bar{T}}P' = 0, \tag{41}$$

in which $p'(x,t) = P'(x)exp(i\omega t)$. An exponential temperature gradient, as an extension of the work of Karimi et al. [33] was considered here. Following Sujith et al. [29] the mean temperature distribution along the duct is given by

$$\bar{T} = Wexp(-mx), \tag{42}$$

where W and m are constants. Sujith et al. [29] then introduced a new independent variable z defined as

$$z = \frac{2\omega}{m\sqrt{\gamma R\bar{T}}}. \tag{43}$$

Substituting Eqs. (42) and (43) into Eq. (41) then yields

$$\frac{d^2P'}{dz^2} + \frac{1}{z}\frac{dP'}{dz} + P' = 0, \tag{44}$$

which is a zeroth order of Bessel equation and its general solution is of the form of

$$P' = [a_1 J_1\left(\frac{\omega\delta}{\sqrt{\theta}}\right) + a_2 Y_1\left(\frac{\omega\delta}{\sqrt{\theta}}\right)], \tag{45}$$

where, J_1 and Y_1 are Bessel and Neumann functions, while δ is a constant given by the following expression,

$$\delta = 2/(m\sqrt{\gamma R}). \tag{46}$$

By applying the linearized momentum equation (Eq. (5)), it can be demonstrated that the acoustic velocity perturbation is expressed by [29]

$$U'(x) = \frac{\omega\delta}{2\sqrt{\bar{T}}}[a_1(J_0\left(\frac{\omega\delta}{\sqrt{\bar{T}}}\right) - J_2\left(\frac{\omega\delta}{\sqrt{\bar{T}}}\right)) + a_2(Y_0\left(\frac{\omega\delta}{\sqrt{\bar{T}}}\right) - Y_2\left(\frac{\omega\delta}{\sqrt{\bar{T}}}\right))]. \tag{47}$$

In this equation, a_1 and a_2 are given by the boundary conditions which are derived from the problem configuration. Assuming that the incident acoustic wave of ε in Fig. 1 features an associated velocity perturbation in the form of

$$U'(0) = \kappa. \tag{48}$$

where κ is a constant velocity amplitude. The configuration of the combustor is assumed as an infinitely long ducts at the both ends of the temperature varying region. The mean temperatures in these two semi-infinite ducts are constant and equal to those at the ends of the temperature varying part (see Fig. 1). Hence, the homogeneous wave equation remains valid in these two regions. Further, due to the lack of reflection the propagating wave in the downstream semi-infinite duct contains only the right travelling component, which is expressed as

$$P'(x) = H.exp(i\omega x/c_L), \tag{49}$$

and

$$U'(x) = (\frac{H}{\bar{\rho}_L\bar{c}_L}).exp(i\omega x/c_L) \tag{50}$$

in which H is a complex constant, $\bar{\rho}$ is a mean density and $\bar{c}$ is a mean sound speed. In Fig. 1, the temperature does not jump at the interface of the semi-infinite duct and the temperature varying part. Hence, the pressure and velocity perturbations at the infinitesimal upstream and downstream of the interface are the same, i.e.

$$P'(L_-) = P'(L_+), \quad U'(L_-) = U'(L_+) \tag{51}$$

Combining Eq. (49) with the solution of the homogeneous wave equation in the downstream semi-infinite part of Fig. 1 renders the anechoic boundary condition

$$p'(L,t) = \bar{\rho}_L\bar{c}_L u'(L,t). \tag{52}$$

Eqs. (48) and (52) then allow the evaluation of the constants $a_1$and a_2 in Eqs. (45) and (47) as given by in Appendix A.

In a homogeneous and one dimensional medium, a solution of the form $p'(x,t) = f(-kx + \omega t) + g(kx + \omega t)$ satisfies the wave equation and identifies the left and right travelling characteristics. By applying such solution in the homogenous parts at either side of the inhomogeneous region (Fig. 1), the pressure and velocity perturbations can be found. At $x = 0$ they are

$$P'(0) = \varepsilon + P_c^-, \quad U'(0) = \frac{1}{\bar{\rho}_0\bar{c}_0}(\varepsilon - P_c^-), \tag{53}$$

and similarly at the end of the region

$$P'(L) = P_c^+, \quad U'(L) = \frac{1}{\bar{\rho}_L \bar{c}_L}(P_c^+). \tag{54}$$

where ε, P_c^- and P_c^+ are respectively the incident, reflected and transmitted acoustic waves. Finally, employing Eqs. (45) and (47) to determine the pressure and velocity at the beginning of the temperature varying region $x = 0$, the ratio of the reflected and incident waves can be written as

$$\frac{P_c^-}{\varepsilon} = \frac{\frac{1}{\sqrt{\theta}}\left[d_1 J_1\left(\frac{\omega\delta}{W}\right) + d_2 Y_1\left(\frac{\omega\delta}{\sqrt{W}}\right)\right] - \rho_0 W\sqrt{\gamma R}}{\left[d_1 J_1\left(\frac{\omega\delta}{\sqrt{W}}\right) + d_2 Y_1\left(\frac{\omega\delta}{\sqrt{W}}\right)\right] + \rho_0 W\sqrt{\gamma R}}. \tag{55}$$

Adopting a similar approach for the transmitted wave renders the following relation for the ratio of the transmitted and incident waves,

$$\frac{p_c^+}{\varepsilon} = 2\frac{\frac{1}{\sqrt{\theta_l}}\left[d_1 J_1\left(\frac{\omega\delta}{\sqrt{\theta_l}}\right) + d_2 Y_1\left(\frac{\omega\delta}{\sqrt{\theta_l}}\right)\right],}{\frac{1}{\sqrt{W}}\left[d_1 J_1\left(\frac{\omega\delta}{\sqrt{W}}\right) + d_2 Y_1\left(\frac{\omega\delta}{\sqrt{W}}\right)\right] + \rho_0\sqrt{\gamma R W}}. \tag{56}$$

2.2.4. Reflected and transmitted wave series

When an incident acoustic wave (ε) enters the combustor, it produces transmitted and reflected waves. The transmitted component propagate through the nozzle ($P_{n,1}^+$) and generates further transmitted and reflected waves ($P_{n,1}^-, P_{n,2}^+ \; and \; P_{n,2}^-$). The reflection of the nozzle ($P_{n,1}^- or \; P_{n,2}^-$) travels back into the combustor and this acts as a new incident wave and the preceding process is repeated forming a series of events. The reflected wave from the nozzle travels into the combustor. It, then, experiences the inverse temperature gradient compared to the incident wave. Due to the linearity of the system, the response of the combustor becomes:

$$Transmission = R_{t,c}(\varepsilon) + R_{t,c}\big(R_{r,n}(R_{t,c}(\varepsilon))\big) + \cdots, \tag{57}$$

$$Reflection = R_{r,c}(\varepsilon) + R_{r,c}\big(R_{r,n}(R_{t,c}(\varepsilon))\big) + \cdots. \tag{58}$$

where subscripts of n, c, r and t denote nozzle, combustor, reflected and transmitted responses, respectively. For the nozzle

$$Transmission = R_{t,n}(R_{t,c}(\varepsilon)) + R_{t,n}(R_{t,c}(R_{r,n}(R_{t,c}(\varepsilon)))) + \cdots, \tag{59}$$

$$Reflection = R_{r,n}(R_{t,c}(\varepsilon)) + R_{r,n}(R_{t,c}(R_{r,n}(R_{t,c}(\varepsilon)))) + \cdots \tag{60}$$

in which $R_{t,c}(\varepsilon) = P_{n,1}^+$. Reflection of the combustor and transmission of the nozzle, series of (58) and (59), will respectively be the total reflection and transmission of the system subject to the acoustic wave (ε). As stated earlier, the reflection and transmission response of the system are developed by the sum of all propagating acoustic waves. The series, therefore, includes infinite terms. Many terms of the series, however, have infinitesimal values. This is due to the light quota of the reflection wave energy of the nozzle traveling upstream compared to energy of the inlet wave [33,34]. In the current work, the terms of series (58) and (59) which are less than 2 percent of the incident wave amplitude (ε) are neglected. In other words, this limit introduces the first term of the truncated series of the transmissions or reflections. All the calculations were done assuming an exponential temperature gradient. In reality, the process of reflection and transmission continues many times and in each reflection the amplitude of the reflected wave decreases. It is therefore, reasonable, to say that at certain stage the amplitude becomes negligible and the process effectively stops. Determination of this threshold is, somehow, subjective. In the current work, the terms of series (58) and (59) which are less than 2 percent of the incident wave amplitude (ε) are neglected. In other words, this limit introduces the first term of the truncated series of the transmissions or reflections. All the calculations were done assuming an exponential temperature gradient.

2.2.5. Validation

To ensure the validity of the relations derived in this section, the following points are considered. (1) When the variation of the stagnation temperature tends to zero (flow becomes adiabatic), the values of A and B in Eq. (16) approach infinity. Under this condition, Eqs. (19) and (20-a) reduce to those of Marble and Candel [25]. Further, Eqs. (22) to (24) are the same as those of Marble and Candel [25] when the Mach number becomes independent of the thermal conditions (i.e. the nozzle becomes adiabatic). In this case, the relations of effective length, Eqs. (36) and (37), reduce to those of Goh and Morgans [19]. (2) Phase change in the second part of a supercritical adiabatic nozzle with an acoustic incident wave is calculated and compared with the results of Goh and Morgans [19] in Fig. 3. The results show complete coincidence, as the relations of (39) and (40) approach those of Goh and Morgans [19] in the limit of adiabatic nozzle.

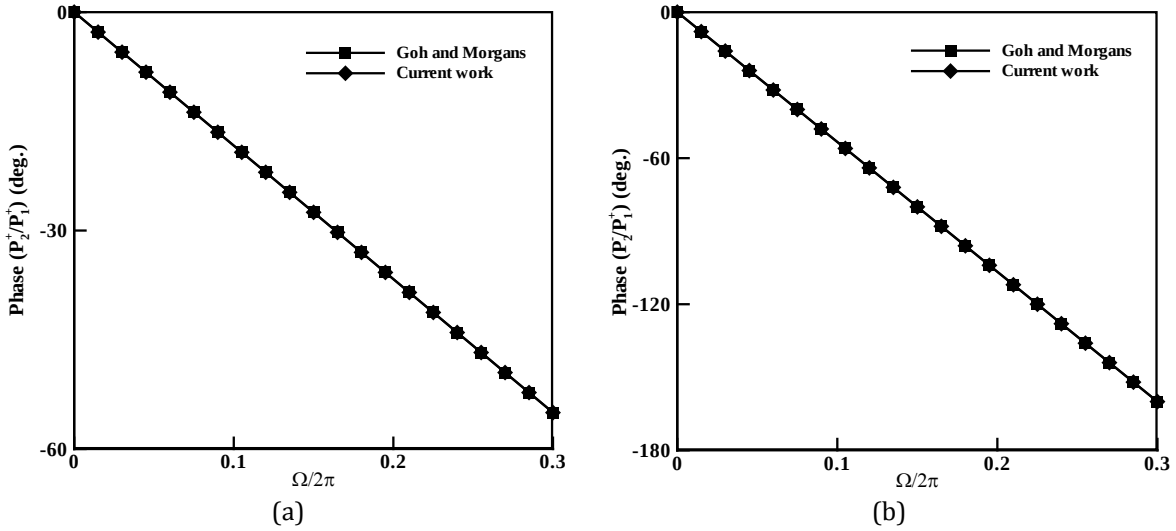

Fig. 3. Phase of the transmitted wave in an adiabatic supercritical nozzle subject to an incident acoustic wave: (a) P_2^+/P_1^+,(b) $\frac{P_2^-}{P_1^+}$, comparison with the results of Goh and Morgans [19].

(3) The phase change in a nozzle (relations (39) and (40)) with no cross-sectional variation should be identical to those derived for a duct, i.e. relations (55) and (56). Fig. 4 illustrates comparison between these for the transmission wave (ε) when the cooling ratio is 0.5. This figure depicts good agreement.

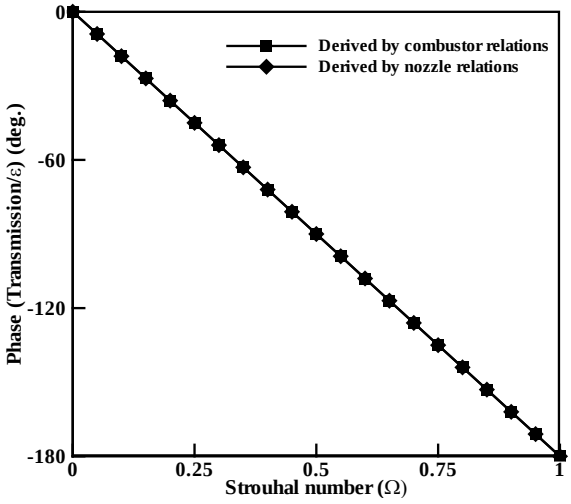

Fig. 4. The acoustic phase change derived by the nozzle relations with no cross-sectional variation and

that of a duct (combustor).

This series of evidence serve as the validation of the current work.

3. Results and discussions

6.1. Compact combustor and nozzle

Figs. 5 and 6 show respectively the total reflection and transmission response of the system subject to an incident acoustic wave for the subcritical and supercritical nozzle conditions. The horizontal axis in this figure represents the nozzle outlet to the combustor inlet stagnation temperature ratio (θ). This figure also contains the results of Marble and Candel [25], which are independent of the variations in the stagnation temperature because of the assumption of an adiabatic flow. The reflection observed is caused by the temperature change along the duct and nozzle as well as the area change through the nozzle. Accordingly, when the system is adiabatic, the responses reduce to that of the exit adiabatic nozzle only. As Figs. 5 and 6 show, in this statue (overall θ=1), the results tend to those of Marble and Candel [25], which further confirm the validity of the relations derived for the nozzle. As these figures describe, by increasing cooling, the reflection is subsided, while the transmission is raised. Heat transfer from the system appears to act as a mechanism of sound generation [34]. In keeping with the existing works, the transmission appreciates by increasing the cooling [33, 34]. The reflected component, however, propagates towards the opposite direction, senses a positive temperature gradient and demonstrates an inverse trend compared to the transmission [33]. The decrement is about 45 percent for both cases 1 and 3 (the inlet nozzle Mach number of 0.05) by 37 percent reduction in the overall θ. This is, however, 38 percent for case 2 and 4 (the inlet nozzle Mach number of 0.1). The transmission illustrates respectively an increment of more than 500 and 300 percent in case 1 and 3. For the case 2 and 4, somewhat 600 and 400 percent growth is observed. Accordingly, the response value is more altered by cooling when a subcritical nozzle is attached at the system outlet. It is clear that variation of the transmission by cooling is much larger than the reflection. Furthermore, the reflection response is more intensive for lower inlet Mach number of the nozzle. The response for the inlet nozzle Mach number of 0.05 could be higher than that of 0.1 up to 12 and 21 percent for reflection and transmission, respectively. This is highlighted at lower values of the overall θ.

The transmission amplitude is higher in comparison to the system reflection in all studied cases. The transmission value is found to be higher in subcritical nozzle regime compared to that of the supercritical condition, while the reflection value is lower. Similarly, the variation range of transmission against heat transfer is higher for subcritical nozzle condition in comparison to the supercritical nozzle condition, while variation range of the reflection is somewhat lower. For instance, the transmission range of case 2 is higher up to 40 percent than that of case 4 by changing through the studied overall θ. Nonetheless, the reflection range of case 2 is lower compared to the case 4 up to 16 percent. Figs. 5 and 6 further depict that all the responses feature monotonic trends.

.

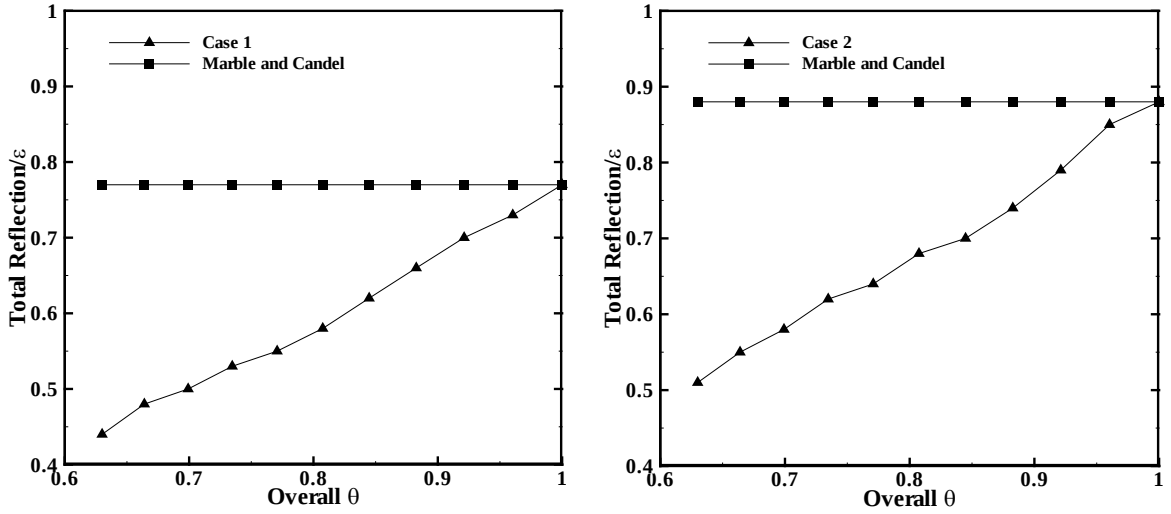

(a)

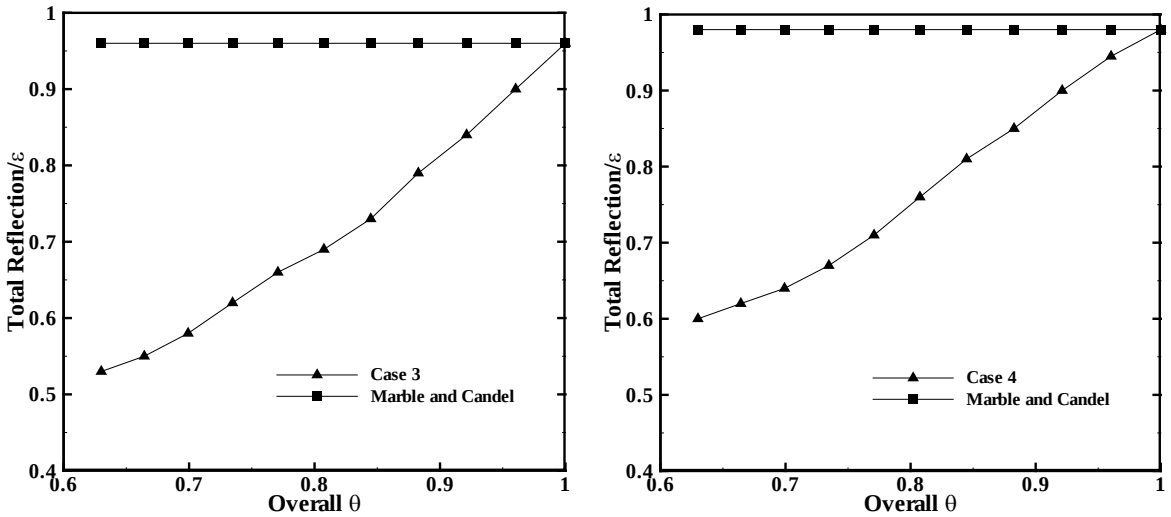

(b)

Fig. 5. Total reflection response of the system per incident acoustic wave for compact combustor and nozzle; (a) subcritical nozzle, (b) supercritical nozzle

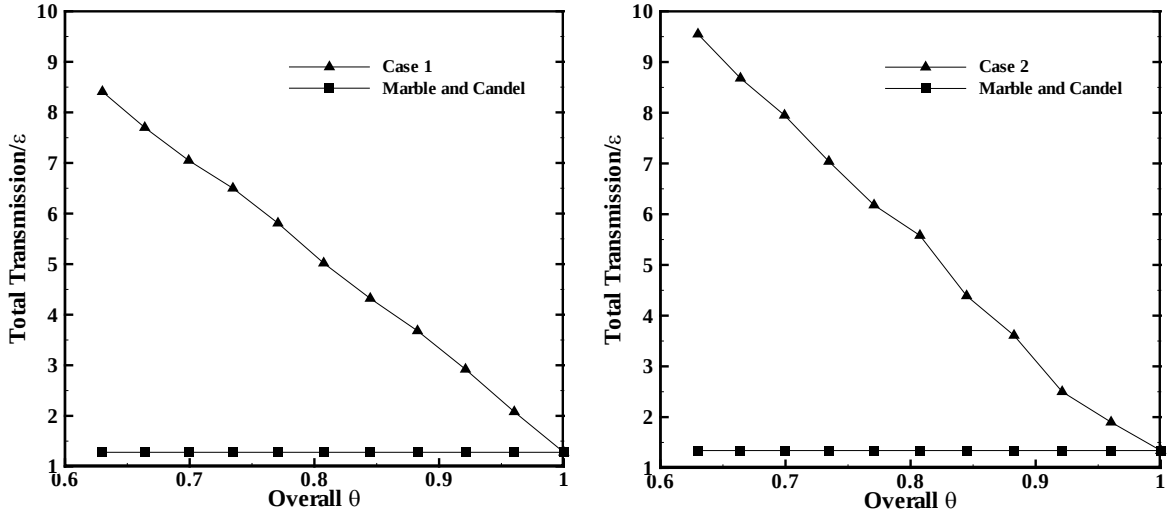

(a)

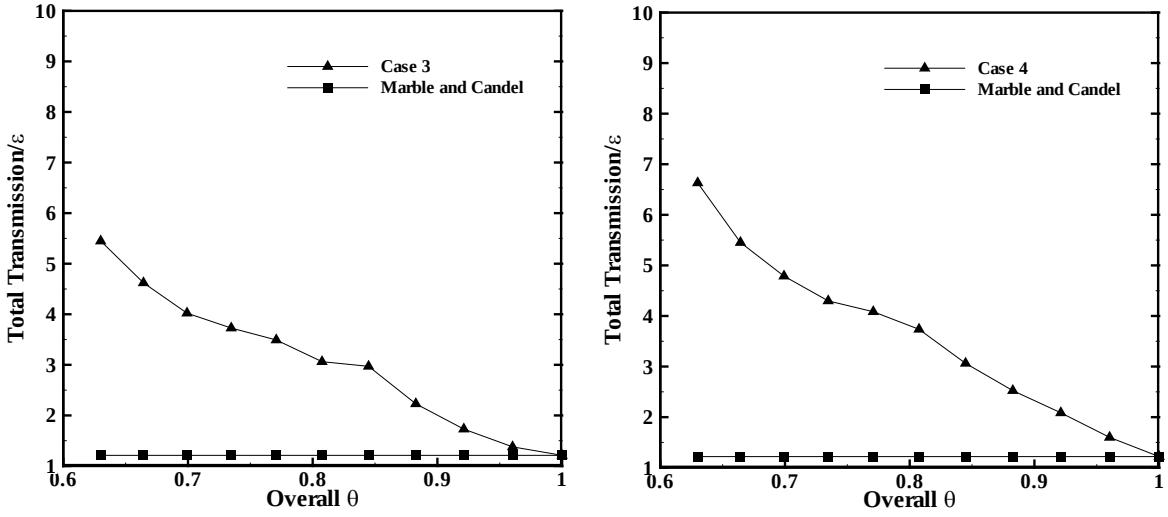

(b)

Fig. 6. Total Transmission response of the system per incident acoustic wave for compact combustor and nozzle; (a) subcritical nozzle, (b) supercritical nozzle

Next, sum of the acoustic energy reflection (Σ_R) and transmission (Σ_T) coefficients, as given in Ref. [34], is calculated. This is

$$|\Sigma_R + \Sigma_T| = \frac{(1-\bar{M}_0)^2}{(1+\bar{M}_0)^2}\left|\frac{p_c^-}{\varepsilon}\right|^2 + \frac{A_1\bar{\rho}_0\bar{c}_0(1+\bar{M}_2)^2}{A_0\bar{\rho}_2\bar{c}_2(1+\bar{M}_0)^2}\left|\frac{p_c^+}{\varepsilon}\right|^2, \quad (61)$$

M, A, c and ρ are the Mach number, cross sectional area, sound speed and density, respectively. The indices 0 and l indicate the inlet and outlet of the combustor or nozzle.

Fig. 7 illustrates the total acoustic energy generated in the system. It is clear from this figure that the acoustic energy generation is zero for adiabatic system with no mean temperature change. This is to be expected as in such system there is no mechanism of sound generation. However, for non-zero overall mean temperature ratios, acoustic energy is generated. The extent of this is inversely proportional with θ and the generation of acoustic energy remains small for values of θ close to unity. Nonetheless, the finite change in the level of acoustic energy is of significance in analysis of thermoacoustic systems [33].

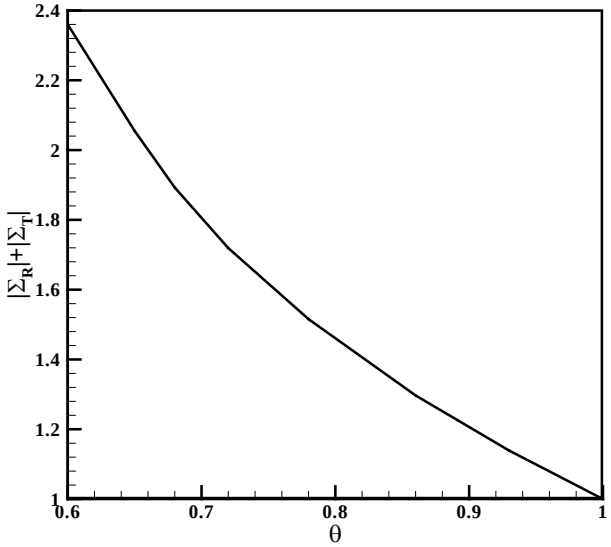

Fig. 7. Sum of the acoustic energy of the reflection and transmission coefficients versus the stagnation

temperature ratio ($\overline{M_0} = 0.1$).

6.2. Non-compact combustor and nozzle

6.2.1. System reflection response

Figs. 8 and 9 illustrate the frequency response of the amplitude of the reflected wave for two thermal condition, and the subcritical and supercritical nozzles, respectively. The amplitude is plotted versus a Strouhal number defined on the basis of the average sound velocity, $\bar{c}$, and the region length, $l + L$. That is,

$$\Omega = \frac{2\omega(l+L)}{\sqrt{\gamma RT_{t,c1}}+\sqrt{\gamma RT_{t,n2}}}. \quad (62)$$

The magnitude of the reflected waves drops from a maximum at zero frequency limit. A series of peaks and troughs are observed. The peaks are slightly higher when the cooling is weakened. The reflection value at the very low frequencies, where the compact assumption holds, is nearly coincided with the results of Fig. 5, which once again expresses a validation of the current analyses. The difference between the two cases shown in each figure becomes negligible by increasing the frequency. This difference, however, is lower for the supercritical nozzle compared with the subcritical nozzle. This shows that the dynamics of the reflection have a minor sensitivity to the Mach number at low values. Nonetheless, as seen for a compact nozzle, the difference becomes more pronounced for lower overall θ and at low frequencies. Reflection approaches to negligible value in lower Strouhal number of the subcritical condition compared to that of the supercritical condition. This behavior is also found for overall θ=0.7 (cases 9 and 10) compared to that of overall θ=0.85 (cases 11 and 12). The reflection shows higher value for a system with supercritical exit nozzle, especially when the cooling is subsided.

Figure 10 shows the phase difference between the total reflected and the incident wave in the supercritical nozzle condition. It is essential to note that the process of acoustic reflection in the current problem involves multiple reflections (see Equation (57)-(60) of the revised manuscript). As stated in our response to the last comment, heat transfer and the resultant density variation in the duct causes some reflection. The change of cross sectional area in the nozzle also induces reflections. Each reflection modifies the phase of the reflected wave. Further, the reflected wave coming back from the nozzle is an incident upstream travelling wave to the duct, which in turn generates a reflection. In reality, this process repeats itself infinite times and the amplitude of the reflected wave becomes progressively smaller. In the current analysis, we have defined a threshold below that we consider the reflection to be negligible. Yet, the total phase presented in the manuscript is the result of many reflection/incident processes that has happened in the system. Thus, the total phase change is the summation of these phase variations as found in the series (58) in the text. That is, essentially, the reason that the phase graph is not well-shaped. An analogous argument applies to the phase of acoustic transmissions shown in Fig. 10. It is inferred from Fig. 10 that the phase change is insensitive to the inlet Mach number of the supercritical nozzle (or the outlet Mach number of the combustor). Cooling, however, can modify the phase difference quite significantly.

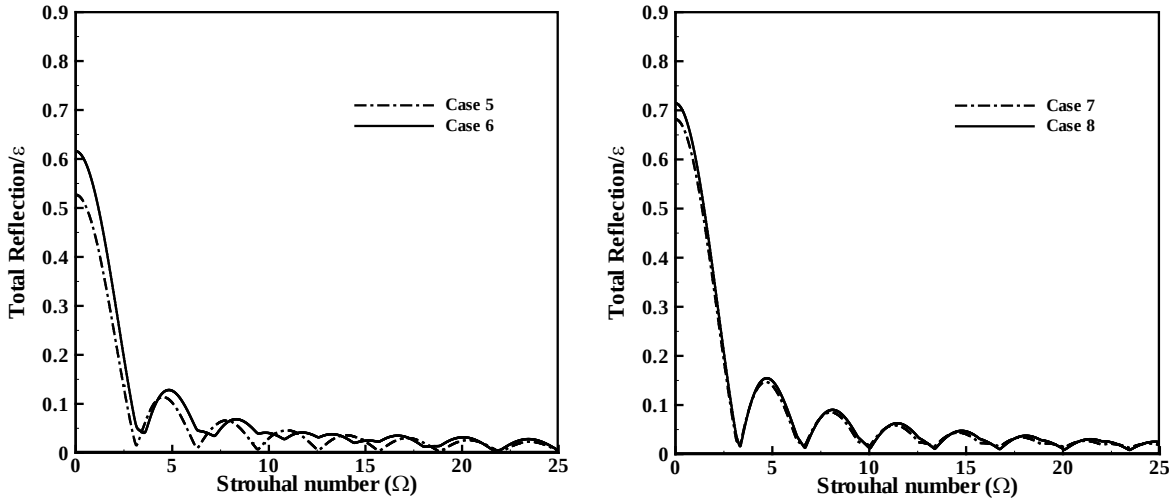

(a) (b)

Fig. 8. Frequency response of the reflected wave per incident acoustic wave for subcritical nozzle and (a) $overall\theta = 0.7$, (b) $overall\theta = 0.85$.

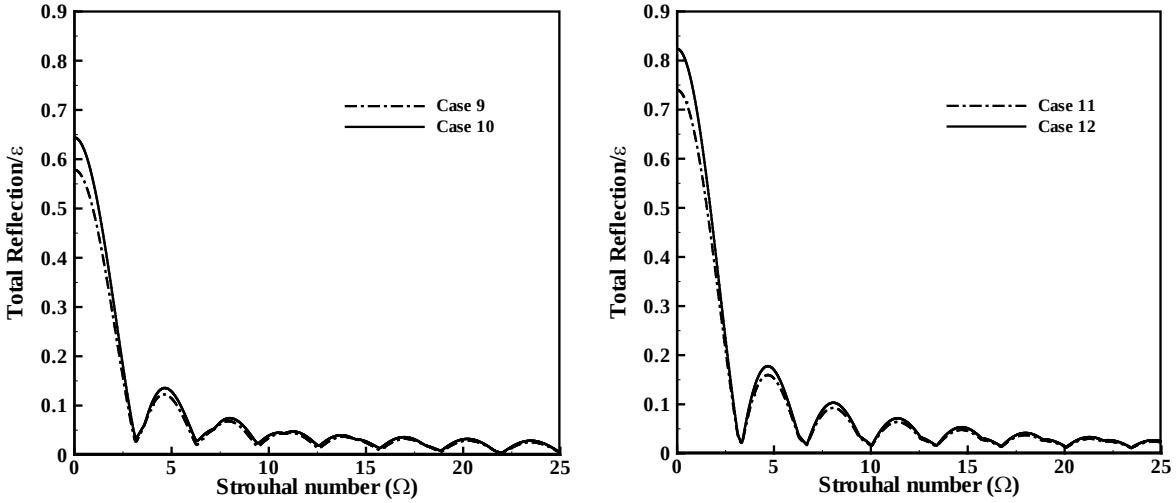

(a) (b)

Fig. 9. Frequency response of the reflected wave per incident acoustic wave for supercritical nozzle and (a) $overall\theta = 0.7$, (b) $overall\theta = 0.85$.

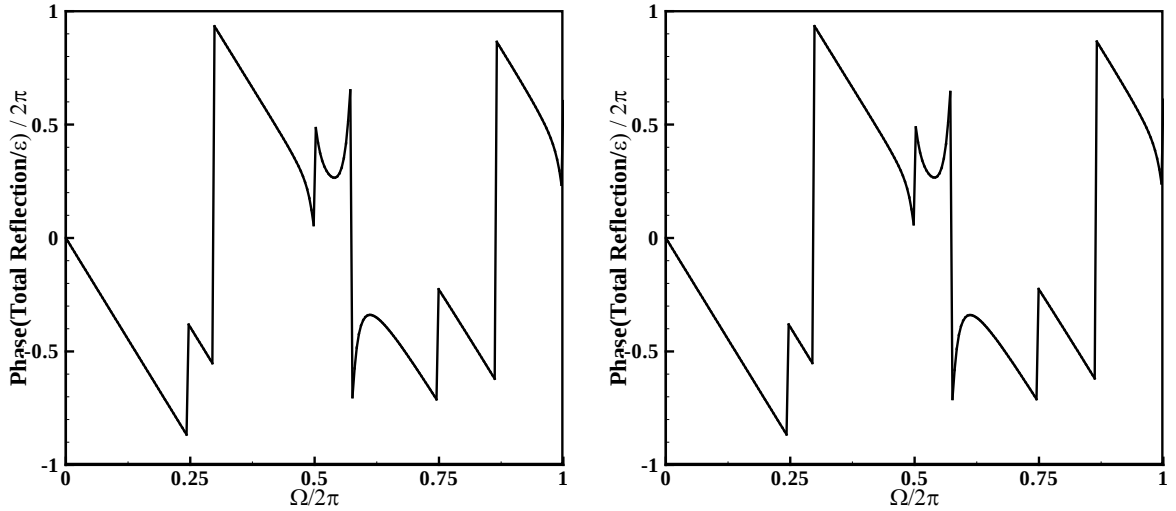

(a) (b)

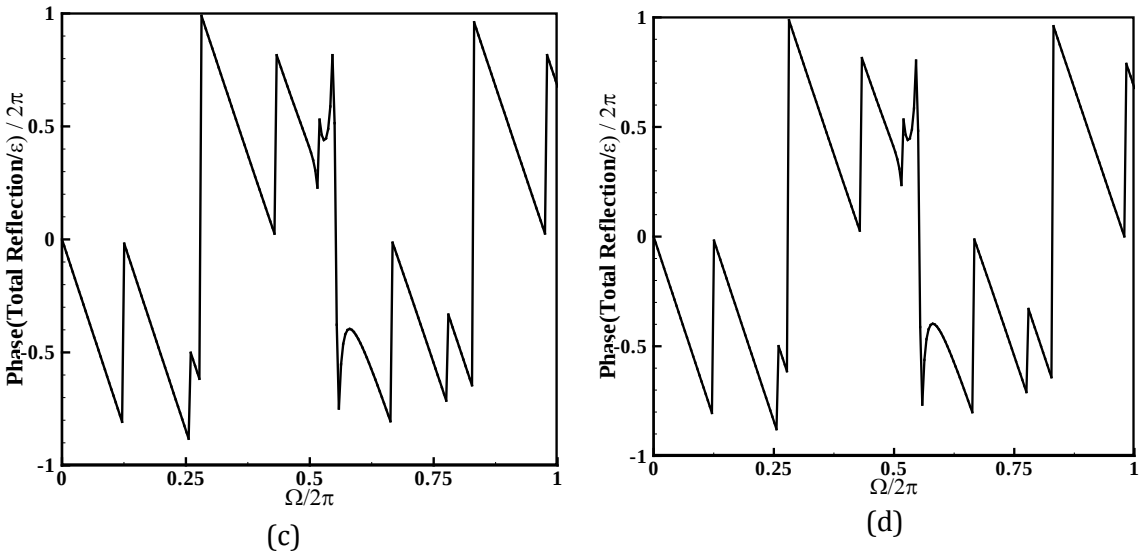

Fig. 10. Phase of the system reflection for supercritical nozzle and different thermal conditions and Mach numbers; (a) case9, (b) case10, (c) case11, (d) case12.

6.2.2. System transmission response

The frequency responses of the transmission coefficient (Figs. 11 and 12) show a trend, which is almost the reverse of that observed in the reflection coefficient (Figs. 8 and 9). These figures show that nearly the full transmission of the incident acoustic wave is seen at the intermediate and high frequencies. Some peaks and troughs are observed at the low frequencies and then the transmission coefficient approaches a constant value. The variation range of the response against frequency variation falls in a narrow band limited to low frequencies. Similar to the compact results, the transmission goes higher by decreasing the Mach number even at the intermediate and high frequencies. This is more highlighted when cooling is intensified. For instance, for subcritical nozzle condition, by decreasing the Mach number from 0.1 to 0.05, the transmission is respectively raised about 13 and 1 percent for the overall θ=0.7 and 0.85. These values for supercritical condition are 16 and 25 percent. Thus, the value of transmission response is lower for supercritical nozzle condition compared to that of the subcritical nozzle condition. Yet, they feature more variation by decreasing the Mach number. Further, cooling can increase the transmission response, especially when a subcritical nozzle is attached at the combustor exit. This increases the transmission about 75 and 36 percent by reducing the overall θ from 0.85 to 0.7 at the Mach number of 0.05 for subcritical and supercritical nozzle, respectively. The transmission response at low frequency again approaches those of the compact combustor and nozzle showed earlier in Fig. 6.

The phase difference between the total transmitted and incident wave is shown in Fig. 13. This is obtained by sum of the phase change between the terms in the series (59), which includes the phase change of the transmitted and incident waves. As can be seen in Fig. 13, cooling and the inlet Mach number of the nozzle (or the outlet Mach number of the combustor) can alter the phase difference. Phase variation falls in the range of 0 to 2π radians for the all investigated cases.

The investigations presented so far indicate that an important parameter influencing the dynamics of sound reflection and transmission is the mean temperature gradient. This quantity may practically vary by either changing the length of the heated/cooled region or altering the temperature difference between the entrance and exit points. The other parameter which

modifies the system response is the Mach number, which can be modified by the changes in the configuration of the combustor and nozzle.

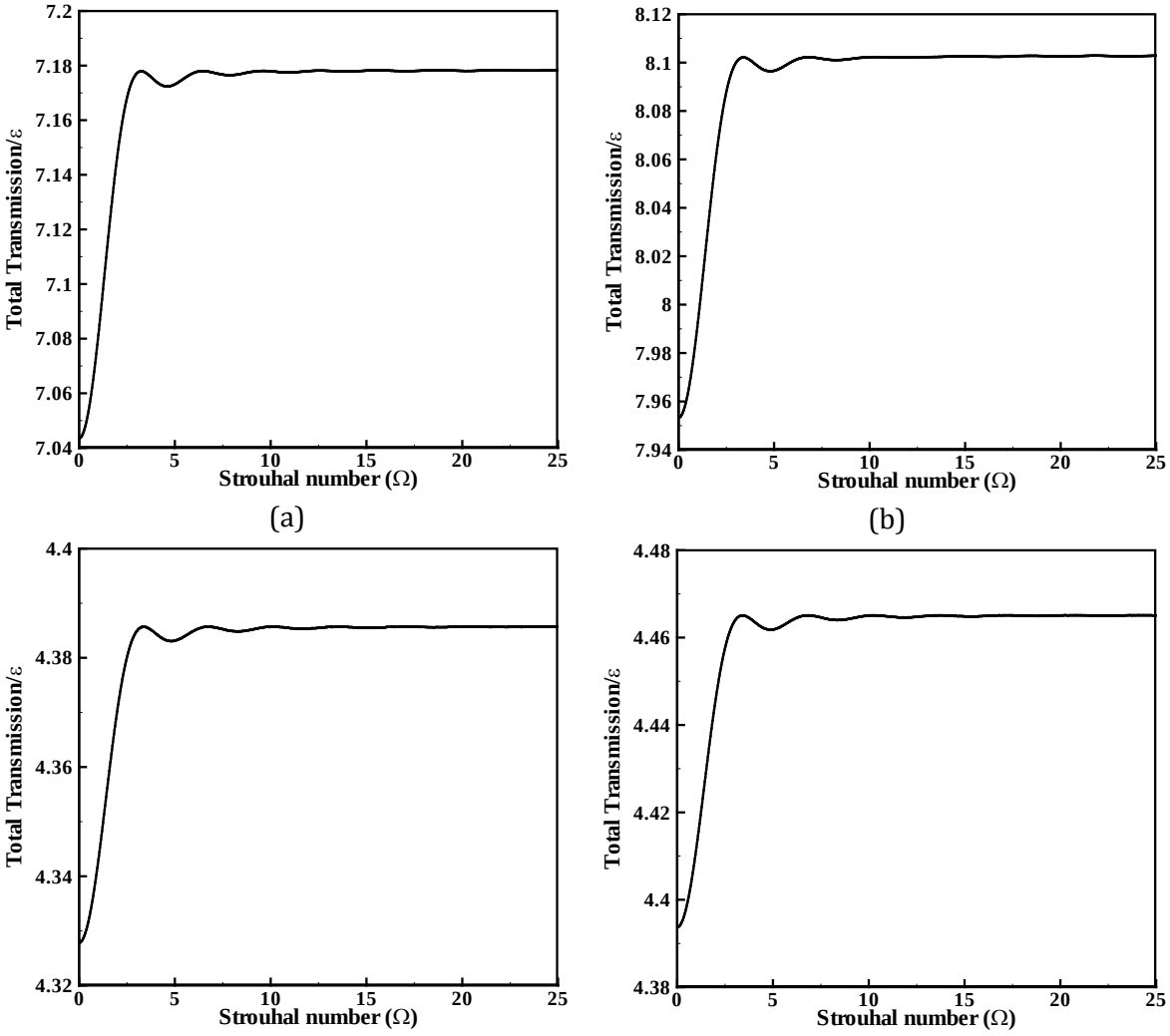

Fig. 11. Frequency response of the transmitted wave per incident acoustic wave for the subcritical nozzle and (a) case5, (b) case 6, (c) case 7, (d) case 8.

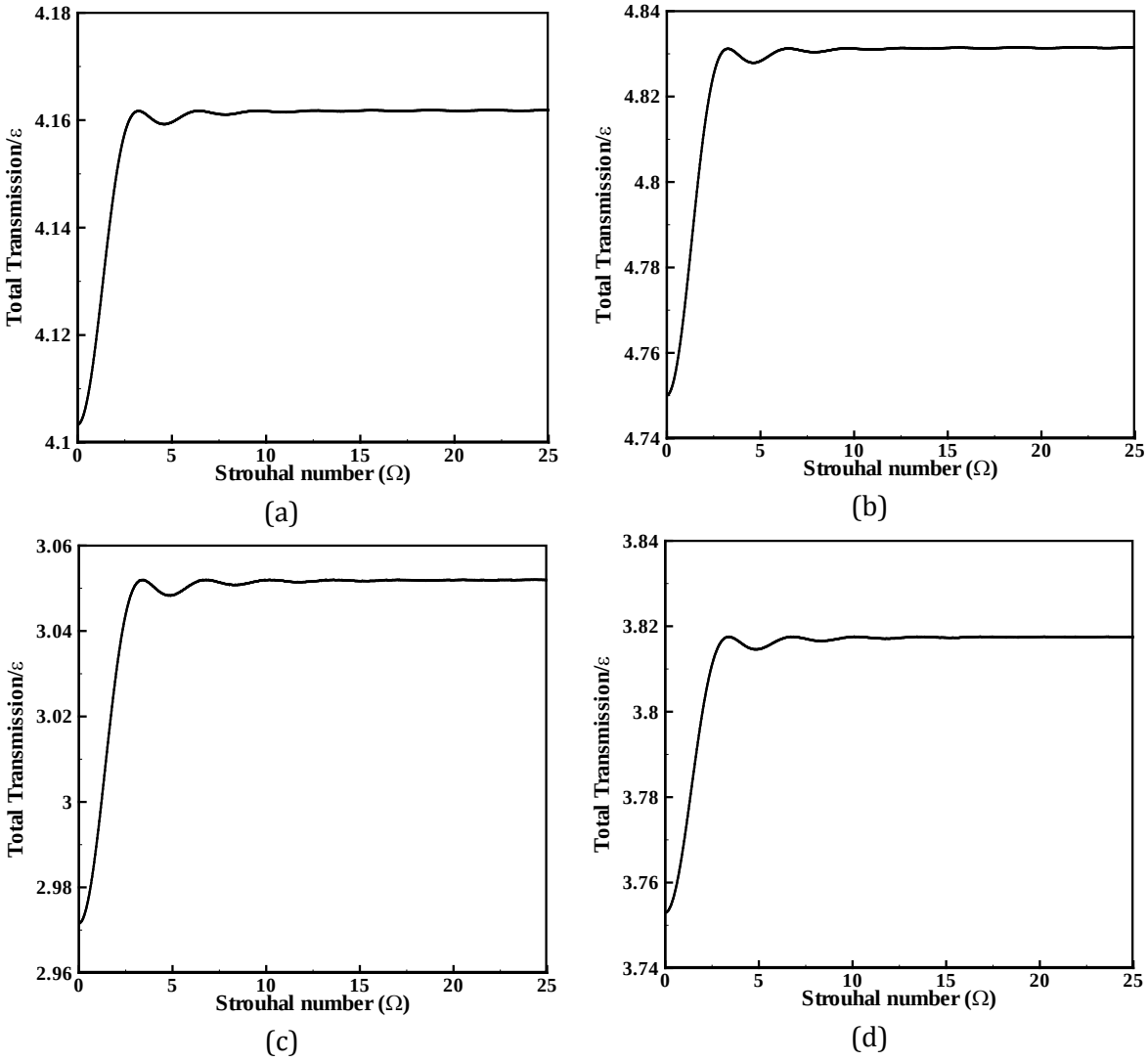

Fig. 12. Frequency response of the transmitted wave per incident acoustic wave for the supercritical nozzle and (a) case 9, (b) case 10, (c) case 11, (d) case 12.

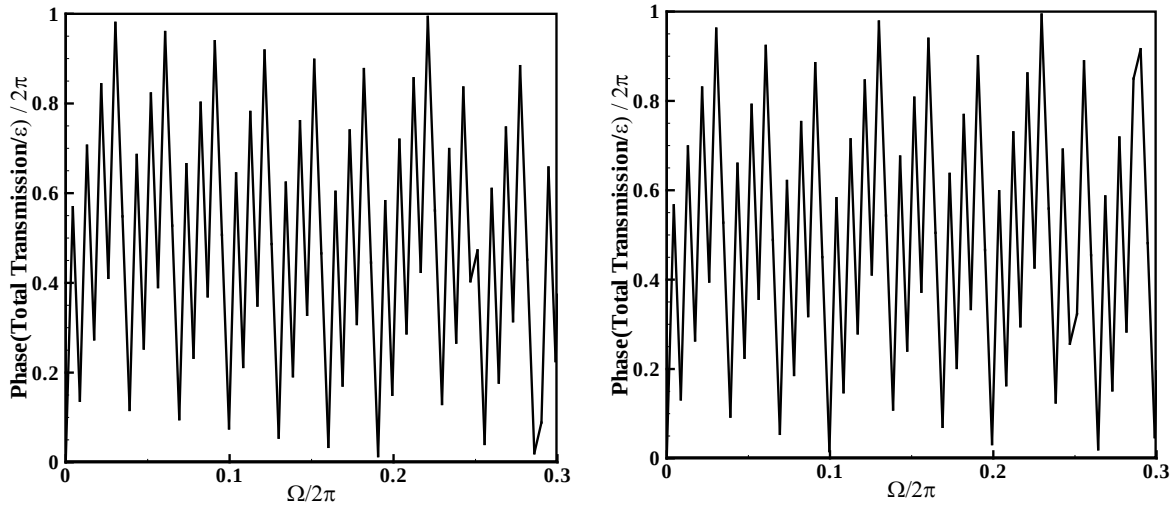

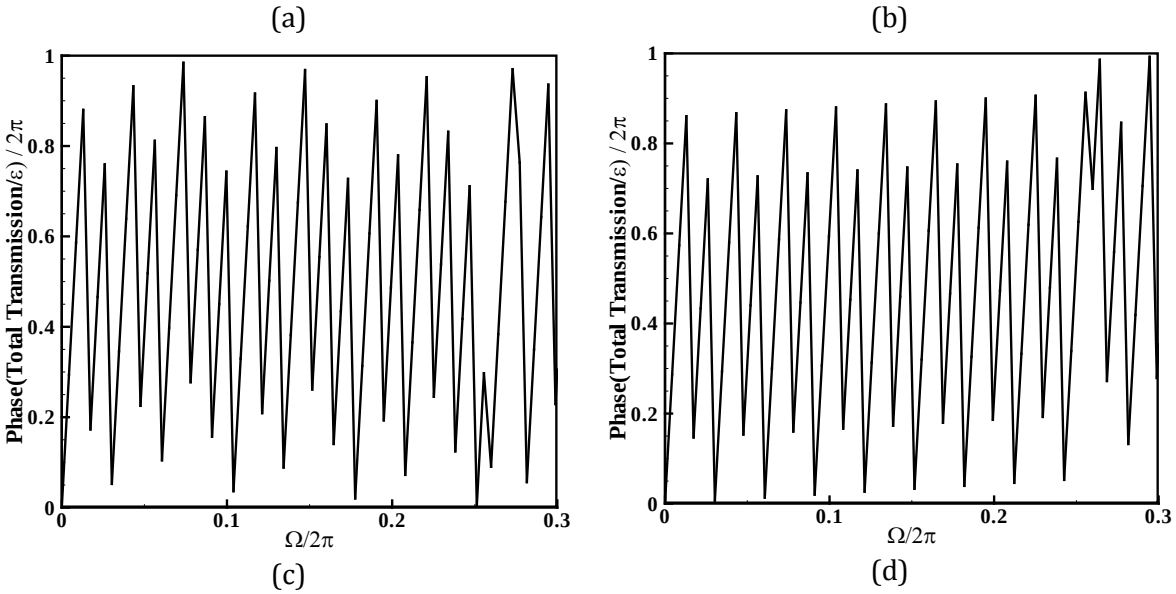

Fig. 13. Phase of the system transmission for the supercritical nozzle and different thermal conditions and Mach numbers; (a) case9, (b) case10, (c) case11, (d) case12.

7. Conclusion

Acoustics of a simplified, non-adiabatic combustor chamber, including a duct followed by a downstream exit nozzle, were considered under an exponential mean temperature distribution. The effect of heat transfer on the dynamics of the acoustic reflection and transmission in the duct and nozzle were investigated analytically. It was demonstrated that the variation in the mean temperature along the system can significantly affect the dynamics of sound refection and transmission.

The main findings of this work can be summarized as follows.

- By increasing cooling, the reflection is subsided, while the transmission is raised.
- The variation of transmission by cooling is much larger than the reflection.
- The response value is more altered by cooling when a subcritical nozzle is attached at the system outlet.
- The transmission amplitude is higher in comparison to the system reflection in all studied cases.
- The phase graph of the system feature a complex and irregular behaviour.
- Phase change is affected by the thermal condition of the system.

References:

[1] T. C. Lieuwen, Unsteady combustor physics. Cambridge University Press, 2012.
[2] T. C. Lieuwen, V. Yang, Combustion instabilities in gas turbine engines (operational experience, fundamental mechanisms and modeling). Progress in astronautics and aeronautics 210(2005).
[3] S. Candel, D. Durox, T. Schuller, N. Darabiha, L. Hakim, T. Schmitt, Advances in combustion and propulsion applications. European Journal of Mechanics-B/Fluids 40 (2013) 87-106.
[4] S. Candel, Combustion dynamics and control: Progress and challenges. Proceedings of the combustion institute 29(1) (2002) 1-28.

[5] H. Ying, V. Yang, Dynamics and stability of lean-premixed swirl-stabilized combustion, Progress in Energy and Combustion Science 35(4) (2009) 293-364.
[6] E. Motheau, F. Nicoud, T. Poinsot, Mixed acoustic-entropy combustion instabilities in gas turbines, Journal of Fluid Mechanics 749 (2014) 542-576.
[7] A P. Dowling, S R. Stow, Acoustic analysis of gas turbine combustors, Journal of propulsion and power 19(5) (2003) 751-764.
[8] S R. Stow, A P. Dowling, Low-order modelling of thermoacoustic limit cycles. ASME Turbo Expo: Power for Land, Sea, and Air. American Society of Mechanical Engineers (2004).
[9] A P. Dowling, A S. Morgans, Feedback control of combustion oscillations. Annual Review of Fluid Mechanics 37 (2005) 151-182.
[10] N. Karimi, Response of a conical, laminar flame to low amplitude acoustic forcing-A comparison between experiment and kinematic theories. Energy 78 (2014) 490-500.
[11] N. Karimi, M. J. Brear, S. H. Jin, J. P. Monty, Linear and non-linear forced response of ducted, laminar premixed flame. Combustion and Flame 156 (2009) 2201-2212.
[12] C. A. Armitage, A. J. Riley, R. S. Cant, A. P. Dowling, S. R. Stow, Flame transfer function for swirled LPP combustion from experiments and CFD. ASME Turbo Exp: Power for Land, Sea, and Air. American Society of Mechanical Engineers (2004).
[13] C. A. Armitage, R. Balachandran, E. Mastorakos, R. S. Cant, Investigation of the nonlinear response of turbulent premixed flames to imposed inlet velocity oscillations. Combustion and Flame 146(3) (2006) 419-436.
[14] M. Shahi, J. B.W. Kok, J.C. R. Casado, A. K. Pozarlik, Assessment of thermoacoustic instabilities in a partially premixed model combustor using URANS approach, Applied Thermal Engineering 71 (2014) 276-290.
[15] P. H. Santosh, T. Lieuwen, Dynamics of laminar premixed flames forced by harmonic velocity disturbances. Journal of Propulsion and Power 24(6) (2008): 1390-1402.
[16] K. Rahul, K. Balasubramanian, R. I. Sujith, Non-normality and its consequences in active control of thermoacoustic instabilities. Journal of Fluid Mechanics 670 (2011): 130-149.
[17] N. Noiray, D. Durox, T. Schuller, S. Candel, A unified framework for nonlinear combustion instability analysis based on the flame describing function. Journal of Fluid Mechanics 615 (2008) 139-167.
[18] W.H. Moase, M.J. Brear, C. Manzie, The forced response of choked nozzles and supersonic diffusers. Journal of Fluid Mechanics 585 (2007) 281-304
[19] CS. Goh, AS. Morgans, Phase prediction of the response of choked nozzles to entropy and acoustic disturbances. Journal of Sound and Vibration 330 (2011) 5184-5198
[20] M. Huet, A. Giauque, nonlinear model for indirect combustion noise through a compact nozzle. Journal of Fluid Mechanics 733 (2013) 268-301
[21] CS. Goh, AS. Morgans, The Influence of Entropy Waves on the Thermoacoustic Stability of a Model Combustor. Combustion Science Technology 185 (2013) 249-268.
[22] M. Leyko, F. Nicoud, T. Poinsot, Comparison of direct and indirect combustion noise mechanisms in a model combustor. AIAA Journal 47(11) (2009) 2709-2716.
[23] I. Durán, S. Moreau, T. Poinsot, Analytical and numerical study of combustion noise through a subsonic nozzle. AIAA journal 51(1) (2012) 42-52
[24] A. D. Pierce, Acoustics: an introduction to its physical principles and applications. Melville, NY: Acoustical Society of America, 1991.
[25] F E. Marble, S M. Candel, Acoustic Disturbances From Gas Non-Uniformities Convected Through a Nozzle. Journal of Sound and Vibration 55(2) (1977) 225-243.
[26] I. Duran, S. Moreau, Solution of the quasi-one-dimensional linearized Euler equations

using flow invariants and the Magnus expansion. Journal of Fluid Mechanics 723 (2013) 190-231.
[27] S M. Candel, F. Defillipi, A. Launay. Determination of the inhomogeneous structure of a medium from its plane wave reflection response, part I: A numerical analysis of the direct problem. Journal of Sound and Vibration 68(4) (1980) 571-582.
[28] S. M. Candel, F. Defillipi, and A. Launay. Determination of the inhomogeneous structure of a medium from its plane wave reflection response, part II: A numerical approximation. Journal of Sound and vibration 68(4) (1980) 583-595.
[29] R. I Sujith, G. A. Waldherr, B. T. Zinn. An exact solution for one-dimensional acoustic fields in ducts with an axial temperature gradient. Journal of Sound and Vibration 184(3) (1995) 389-402.
[30] R. I. Sujith, Exact solutions for modeling sound propagation through a combustion zone. The Journal of the Acoustical Society of America 110(4) (2001) 1839-1844.
[31] B. Karthik, B. M. Kumar, R. I. Sujith, Exact solutions to one-dimensional acoustic fields with temperature gradient and mean flow. The Journal of the Acoustical Society of America 108(1) (2000) 38-43.
[32] B. Karthik, R. Krishna Mohanraj, R. Ramakrishnan, R. I. Sujith, Exact solution for sound propagation in ducts with an axial mean temperature gradient and particulate damping. The Journal of the Acoustical Society of America 106(5) (1999) 2391-2395.
[33] N. Karimi, M. Brear, W. Moase, Acoustic and disturbance energy analysis of a flow with heat communication. Journal of Fluid Mechanics 597 (2008) 67-89.
[34] N. Karimi, M. Brear, W. Moase, On the interaction of sound with steady heat communicating flows. Journal of Sound and Vibration 329 (22) (2010) 4705-4718.
[35] M. Leyko, S. Moreau, F. Nicoud, T. Poinsot, Numerical and analytical modeling of entropy noise in a supersonic nozzle with a shock, Journal of Sound and Vibration 330 (2011) 3944-3958.
[36] J. E. John, G K. Theo, Gas Dynamics. Pearson Prentice Hall, 2006
[37] AH. Shapiro, The Dynamics and Thermodynamics of Compressible Fluid Flow, New York, The Ronald Press Company, 1953.
[38] S.R. Stow, A.P. Dowling, T.P. Hynes, Reflection of circumferential modes in a choked nozzle, Journal of Fluid Mechanics 467 (2002) 215-239.
[39] I. Duran, S. Moreau, Solution of the quasi-one-dimensional linearized Euler equations using flow invariants and the Magnus expansion, Journal of Fluid Mechanics 723 (2013) 190-231.

Appendix A

For an exponential temperature distribution, the coefficients a_1 and a_2, in Eqs. (55) and (56) are given by

$$a_1 = \frac{E}{EH-FG}, a_2 = \frac{F}{EH-FG} \quad \text{(A-1)}$$

in which E, F, G and H are

$$E = J_1\beta_l - f\alpha_l J_1(\beta_l) - f\lambda_l J_0(\beta_l) + f\lambda_l J_2(\beta_l) \quad \text{(A-2)}$$

$$F = Y_1\beta_l - f\alpha_l Y_1(\beta_l) - f\lambda_l Y_0(\beta_l) + f\lambda_l Y_2(\beta_l) \quad \text{(A-3)}$$

$$G = \alpha_0 J_1(\beta_0) + \lambda_0 J_0(\beta_0) - \lambda_0 J_2(\beta_0) \quad \text{(A-4)}$$

$$H = \alpha_0 Y_1(\beta_0) + \lambda_0 Y_0(\beta_0) - \lambda_0 Y_2(\beta_0) \quad \text{(A-5)}$$

In the above relations $\alpha_0, \alpha_1, \beta_0, \beta_1, \lambda_0, \lambda_1$ and f depend on the mean temperature and the forcing frequency; see Eq. (46) for definition of δ.

$$\alpha_0 = \frac{mW^{-1/2}i}{2\omega\rho_l}, \beta_0 = \frac{\omega\delta}{\sqrt{W}}, \lambda_0 = \frac{\delta ci}{4\delta W\rho_l} \ , \tag{A-6}$$

$$\alpha_1 = \frac{mT_l^{-1/2}i}{2\omega\rho_l}, \beta_1 = \frac{\omega\delta}{\sqrt{T_l}}, \lambda_1 = \frac{\delta ci}{4\delta T_l\rho_l}, \tag{A-7}$$